Mon. Not. R. Astron. Soc. **277,** 1177–1184 (1995)

Including the effect of gravitational light bending in X-ray profile modelling

D. A. Leahy and L. Li

Department of Physics, University of Calgary, 2500 University Dr. N. W., Calgary, Alberta T2N 1N4, Canada

Accepted 1995 July 25. Received 1995 July 25; in original form 1995 May 26

ABSTRACT

The purpose of this work is to generalize pulse shape modelling to include the effect of light bending due to general relativity. A simple analytical formula is found to describe the light-bending effect accurately, and is incorporated into the emission model for calculation of the pulse shapes from rotating accreting neutron stars. Least-squares fittings are performed to a subset of pulsars studied by Leahy. The fittings with light bending show significant improvement over the fittings without light bending, and the resulting derived emission region geometry gives narrower rings, as expected on theoretical grounds. The model is also applied to the transient pulsar EXO 2030 + 375. The relation between the luminosity and the properties of the emission rings is studied. For this pulsar we conclude that some effect other than changing emission ring size is responsible for the change in pulse shape.

Key words: relativity – pulsars: individual: EXO 2030 + 375 – stars: neutron – X-rays: stars.

1 INTRODUCTION

Under current theories, X-ray pulsars are assumed to be rotating magnetic neutron stars. A binary X-ray pulsar derives its energy from gravitational potential energy released when matter is accreted on to the surface of the neutron star. The presence of a magnetic field around a neutron star strongly influences the accretion mechanism. In the case of a dipole field, the inflowing material will follow the field lines to the neutron star surface and arrive on a region the shape of a ring around each of the magnetic poles. From the interaction of the inflowing material with the magnetosphere of the neutron star, a theoretical estimate of the size of the accretion region can be obtained. The radius of the polar cap on the surface of a neutron star is typically 10^{-1}–$10^{-2} R_*$ (R_* is the radius of the neutron star). This gives a very small polar cap angle of 0°.57–5°.7 (Mészáros 1992). This estimate of the accretion region is much smaller than the results from the simple emission model of Leahy (1991).

By fitting the calculations of the emission model to the observed pulse profiles, Leahy (1991) made the first attempt to establish a detailed viewing geometry of the neutron star. The model assumes two emission rings on the surface of the neutron star, each centred about a magnetic axis of the neutron star. The two magnetic axes can be offset by an angle θ_o. The emission from the two rings is assumed to be uniform, and the flux is taken to be one of the following two analytical functions:

$$I(\theta') \cos\theta' = A \cos^2\theta', \quad (1)$$

$$I(\theta') \cos\theta' = A \cos^4\theta'. \quad (2)$$

These two equations are simple approximations (Leahy 1990) to the theoretical calculations of Mészáros & Nagel (1985) for emission by a slab of magnetized plasma. This model was applied to 20 X-ray pulsars. The derived emission regions were relatively large.

Bulik et al. (1992) fitted spectra in 16 pulse phase bins for 4U 1538 – 52, calculating a filled polar cap model with a radiative transfer code. They also found large polar caps, an offset, and significant differences between the caps.

Riffert et al. (1993) used a similar geometry model as Leahy (1991), but took into account corrections from the relativistic light bending near the neutron star. Least-squares fits were performed to three selected pulsars. They assumed the emission regions to have identical shape and size at both magnetic poles, and chose some cap and ring sizes to do the calculations. The best-fitting sizes were significantly smaller compared to the best fits of the non-relativistic model of Leahy (1991). Based on these calculations, they concluded that the relativistic model is more consistent with the theoretical estimates.

In this paper, we find a simple analytical formula to describe accurately the light-bending effect due to general relativity. Through this simple formula, the light-bending

effect is incorporated into the emission model. The light-bending model is applied to seven pulsars to find the best fits. After the light-bending effect is included into the model, the fittings of the model with the observations are improved, and quite different geometry parameters are derived.

2 GRAVITATIONAL LIGHT BENDING

Deflection of light in a gravitational field is presently one of the three experimentally measurable consequences of general relativity. The other two are (1) the redshift, and (2) the perihelion precession of Mercury. Modifications to the gravitational field strength due to general relativity become important when considering the properties of compact objects like neutron stars. Indeed, it is largely for this reason that compact objects are of such great theoretical interest.

In neutron stars, the neutrons are degenerate and provide the necessary opposition to the gravity forces. Based on this theory, the mass and radius of a neutron star can be estimated from the models of the equation of state. For the current models (Shapiro & Teukolsky 1983), the radius of a neutron star, r_0, is approximately in the range $2 \le r_0 \le 4$, where r_0 is in the unit of Schwarzchild radius R_s ($R_s = 2GM/c^2$). In this case, gravitational light bending is expected to occur near the neutron star surface.

Fig. 1 shows the geometry of the light bending near the surface of a neutron star. The thick black line indicates the path of the light. The light is emitted from the neutron star surface at an angle θ' to the local normal. When it reaches the observer, it makes an angle θ'_0 to the normal line. The relation between θ' and θ'_0 is (see Riffert & Mészáros 1988)

$$\theta'_0(r, r_0, \mu) = b \int_{r_0}^{r} \frac{1}{x}\left[x^2 - b^2\left(1 - \frac{1}{x}\right)\right]^{-1/2} \mathrm{d}x, \qquad (3)$$

where

$\mu = \cos\theta'$,

$b = \dfrac{r_0}{A_0}(1-\mu^2)^{1/2}$, the relativistic impact parameter,

$A_0 = \left(1 - \dfrac{1}{r_0}\right)^{1/2}$,

$r_0 = \dfrac{Rc^2}{2GM}$, (the neutron star radius in Schwarzchild units).

We usually take $r \to \infty$ in equation (3) (the observer is at infinity).

The integration of equation (3) has no analytical solution. It is not easy to incorporate into the integration for calculating the angular distribution of flux, since the flux integration itself is long and complicated (see Leahy 1991).

However, from the numerical calculation of equation (3), we find that the relation between $\cos\theta'_0$ and $\cos\theta'$ can be fitted by straight lines. For $r_0 \ge 2$, these straight-line fits are nearly perfect, and the bigger the r_0, the better the fit. (See Fig. 2a for an example with $r_0 = 2.4184$.) $r_0 = 2.4184$ is obtained from the estimated radius and mass of most neutron stars: $R = 10$ km, $M = 1.4\,M_\odot$ (see Mészáros 1992). When $r_0 < 2$, the plots of $\cos\theta'_0$ versus $\cos\theta'$ are obviously curved; linear fits are not very suitable in these cases (see Fig. 2b).

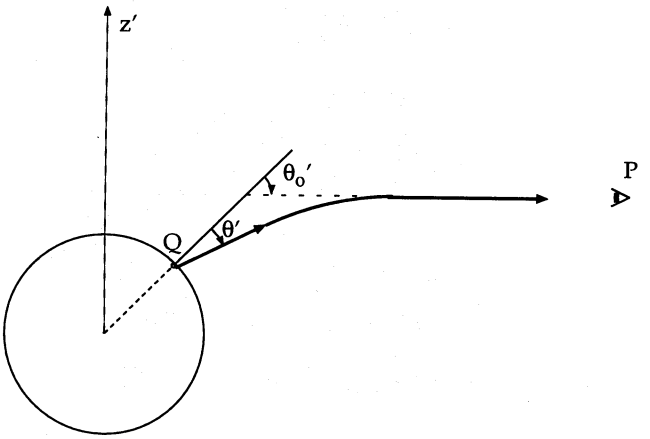

Figure 1. Geometry of the light bending, showing coordinates of emission point Q (r_o, θ'', ϕ'') and the observer point P (r, θ_1, ϕ_1). ($r \to \infty$).

Table 1 lists the slope a and intercept b of the fitted straight lines for different r_0. We can see that a and the absolute value of b become smaller when r_0 increases (see Table 1). r_0 indicates the density of the star, larger r_0 corresponding to smaller density; a and $|b|$ are indications of the gravitational effects; smaller a and $|b|$ mean less gravitational effects in comparison. When r_0 increases, the decrease of the star density will result in smaller modification to general relativity; thus a and $|b|$ will decrease. So strong correlations exist between a and r_0, and between b and r_0. For r_0 in the reasonable range for neutron stars, $2 \le r_0 \le 5$, these correlations can also be very well fitted using very simple formulae (see Fig. 3). When $r_0 > 5$, a and b will deviate from the fitted curve of Figs 3(a) and (b). Thus these fits should be performed separately in different ranges, i.e., the neutron star range, the white dwarf range and the normal star range, etc. In this paper, only the neutron star is of concern; thus the fits for r_0 in the range [2, 5] will be used.

Thus the light-bending equation (3) can be replaced by the following simple equations:

$$\cos\theta'_0 = a \times \cos\theta' + b, \qquad (4)$$

where

$$a = \frac{2.653}{r_0^2} + \frac{0.381}{r_0} + 1.068, \qquad (5)$$

$$b = -\frac{2.944}{r_0^2} - \frac{0.232}{r_0} - 0.087, \qquad (2 \le r_0 \le 5). \qquad (6)$$

3 THE MODEL FITS TO THE PULSAR PROFILES

The light-bending model is applied to seven of the 20 pulsars studied by Leahy (1991), and the results are compared with Leahy's no-light-bending model.

Table 2 lists the fitted parameters from both the no-light-bending model and the light-bending model. Both of the analytical functions for the intensity distribution were used for the model: $I(\theta')\cos\theta' = A\cos^2\theta'$; and $I(\theta')\cos\theta' = A\cos^4\theta'$. Generally, the $\cos^2\theta'$ model will give better fits, especially when the light-bending effect is included. The fits

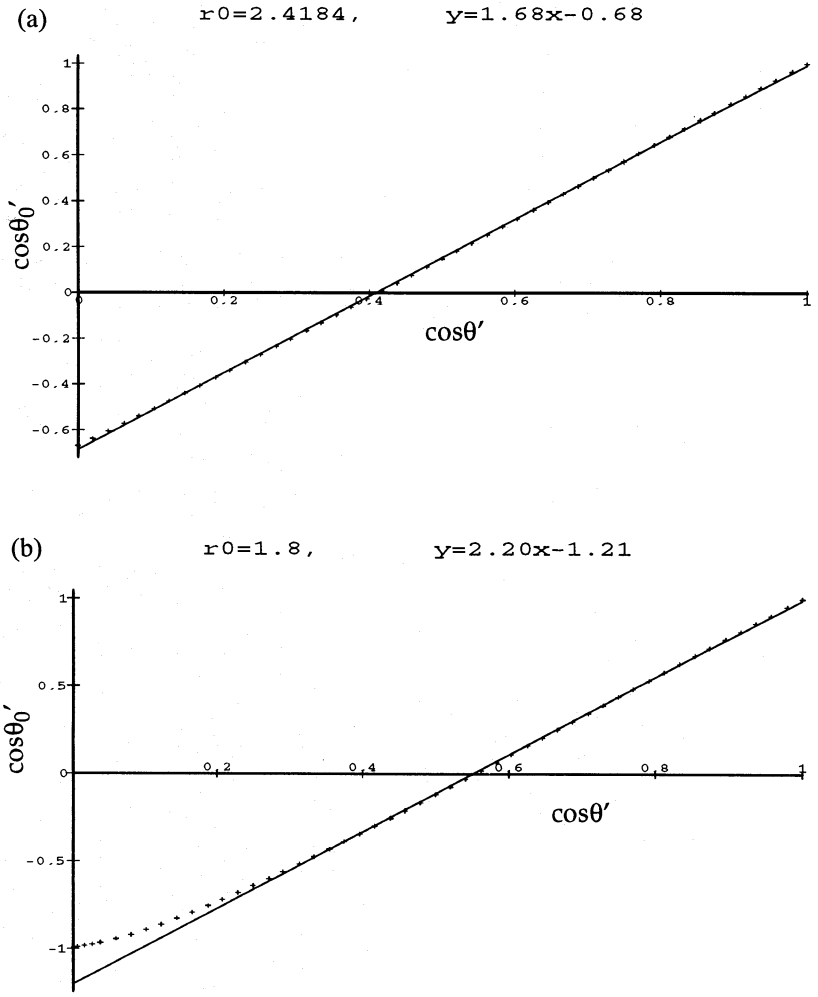

Figure 2. (a) Linear fitting of the light-bending formula (equation 3) for the typical values of neutron star radius: $r_0 = 2.4184$. (b) When $r_0 < 2$, the plot of cos θ_0' versus cos θ is obviously curved, and the data points deviate from a straight line. Linear fitting is not suitable for the full range of cos θ', but still perfect in a smaller range, e.g., [0.3, 1] for $r_0 = 1.8$. (The data points are numerical calculations from equation 3.)

Table 1. Fitted slope a and intercept b for different r_0.

r_0	a	b	r_0	a	b	r_0	a	b
2.0	1.922	-0.942	3.0	1.490	-0.493	4.0	1.330	-0.330
2.2	1.789	-0.800	3.2	1.446	-0.448	4.4008	1.291	-0.292
2.3	1.734	-0.743	3.3	1.427	-0.429	4.6	1.275	-0.276
2.4184	1.678	-0.684	3.4	1.410	-0.411	5.0	1.248	-0.248
2.5	1.642	-0.648	3.5	1.394	-0.395	50.0	1.020	-0.020
2.6	1.604	-0.609	3.6	1.379	-0.380	100	1.010	-0.100
2.8	1.542	-0.545	3.8	1.352	-0.354			

listed in the table are all $\cos^2\theta'$ model, except 4U 1626 − 67, for which the $\cos^4\theta'$ model gives a much better fit. For each object in the table, the first row lists the parameters for the no-light-bending model, while the second row lists the parameters for the light-bending model. The goodness of fit was not determined, because the statistical errors were not available for the majority of the published pulse profiles. However, restricted to a given pulsar, the resulting least sum-of-squares (SSQ) gives a relative measure of goodness of fit for comparing the different models (e.g., the $\cos^2\theta'$ model and the $\cos^4\theta'$ model, the no-light-bending model and the light-bending model, etc.).

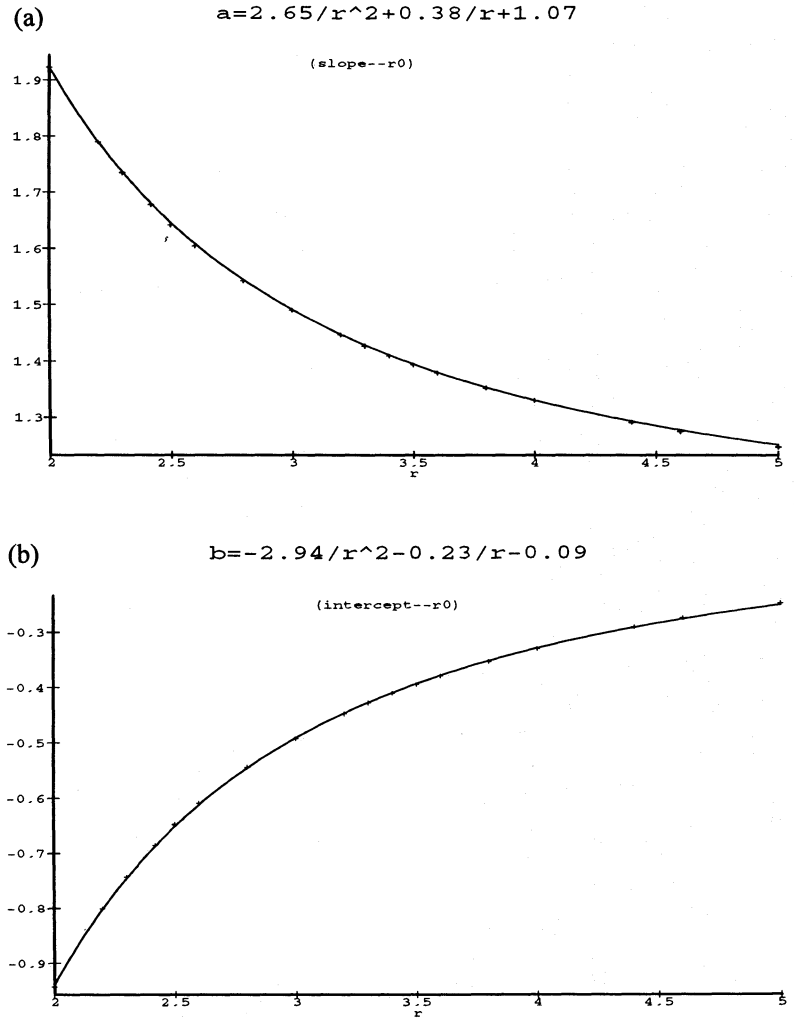

Figure 3. (a) Fitted relation between slope and r_0. (b) Fitted relation between intercept and r_0. ($2 \leq r_0 \leq 5$).

Table 2 also shows the comparison of the two models: the no-light-bending model and the light-bending model, where the solid angle of the neutron star is given by

$$\Omega = \int \sin\theta \, \mathrm{d}\theta \, \mathrm{d}\phi, \tag{7}$$

and the emitting area is $A = \Omega R^2$, with R the radius of the neutron star.

Fig. 4 shows the pulse profiles. We can see that the light-bending model can give better fits to the peaks and dips of the profiles. This is because when the light-bending effect is ignored, θ' is the same as θ'_0, and the radiation pattern is

$$I(\theta') \cos\theta' = B \cos^2\theta' = B \cos^2\theta'_0. \tag{8}$$

The integration over this $\cos^2\theta'_0$ pattern will give relatively flat profiles. The radiation pattern including the effect of light bending is

$$\begin{aligned} I(\theta') \cos\theta' &= B \cos^2\theta' = B(c \cos\theta'_0 + d)^2 \\ &= e \cos^2\theta'_0 + f \cos\theta'_0 + g, \end{aligned} \tag{9}$$

where c, d, e, f and g are constants.

Here, the $\cos\theta'_0$ and the constant term in the radiation pattern can give sharper features in the profile. That is why the profile of the light-bending model is more flexible and can fit the observations better.

4 EXO 2030+375: THE LUMINOSITY DEPENDENCE OF PULSE PROFILE

EXO 2030+375 is a transient X-ray pulsar discovered by Parmar, White & Stella (1989a,b). The observed pulse profiles show strong luminosity dependence. The large luminosity range for an individual pulsar allows for the first time the possibility of investigating how pulse formation varies with luminosity.

We expect that the dependence of the pulse profile on luminosity is caused by the changes in the structure of the accretion disc and its interaction with the magnetosphere of the neutron star. The inflowing plasma will thread different magnetic field lines and fall on to different regions of the neutron star surface. The higher luminosity, which is associated with higher accretion rate, thus higher dynamic pressure, will cause the plasma to fall in on closer field lines

Table 2. Comparison of the two models.

Pulsar [a]	Rotational & magnetic axis angles [b]: θ_m, θ_r	Emission ring angles [b] $\alpha_1, \beta_1, \alpha_2, \beta_2$	Offset angle [b]: θ_o	Solid angle of the emission region: Ω	Comments [e]
4U0115+63 [c]	1.515, 0.530	0.599, 0.622, 0.561, 0.583	0.595	0.1556	SSQ: ↓ 11.2%; Size: ↓ 22.4%;
	1.632, 0.499	0.602, 0.618, 0.562, 0.581	0.007	0.1208	θ_o: ↓ 98.8%.
Cen X-3 [c]	1.461, 0.368	0.287, 0.433, 0.558, 0.602	0.759	0.7299	SSQ: ↓ 52.0%; Size: ↓ 11.7%;
	1.541, 0.415	0.238, 0.444, 0.555, 0.616	0.020	0.6444	θ_o: ↓ 97.4%.
4U1626-67 [d]	0.246, 0.246	0.000E0, 0.068, 0.200, 0.300	0.100	0.1699	SSQ: ↓ 0.6 %; Size: ↓ 6.5%;
	0.320, 0.321	0.13E-4, 0.034, 0.200, 0.300	0.100	0.1589	θ_o: the same.
4U1258-62 [c]	1.252, 0.168	0.465, 0.487, 0.405, 0.428	0.507	0.1207	SSQ: ↓ 20.7%; Size: ↓ 13.8%;
	1.212, 0.118	0.472, 0.482, 0.400, 0.430	0.218	0.1041	θ_o: ↓ 57.0%.
4U0900-40 [c]	1.427, 0.617	0.468, 0.501, 0.357, 0.482	0.172	0.4149	SSQ: ↓ 76.4%; Size: ↓ 5.4%;
	1.407, 0.655	0.411, 0.464, 0.634, 0.292	-0.167	0.3927	θ_o: ↓ 2.9%.
4U1118-61 [c]	0.602, 0.602	0.000E0, 0.035, 0.040, 0.052	0.100	0.0073	SSQ: ↓ 76.8%; Size: ↓ 50.7%;
	0.838, 0.823	0.051, 0.060, 0.056, 0.058	-0.415	0.0036	θ_o: ↑ 315%.
GPS1722-36 [c]	0.851, 0.902	0.488, 0.690, 0.565, 0.770	0.437	1.5009	SSQ: ↓ 9.2%; Size: ↑ 11.0%;
	0.520, 1.269	0.108, 0.740, 0.672, 0.684	0.674	1.6655	θ_o: ↑ 54.2%.

[a]The first row for each object lists parameters for the no-light-bending model; the second row lists parameters for the light-bending model.
[b]The unit for angles is radians.
[c]The intensity distribution used in the models is $\cos^2\theta'$.
[d]The intensity distribution used in the models is $\cos^4\theta'$.
[e]This column compares the light-bending model with the no-light-bending model.
SSQ: Sum of squared deviation.
Size: the area of the emission region, which equals ΩR^2, with R the neutron star radius.
↓: decreased. ↑: increased, on the value of no-light-bending model.

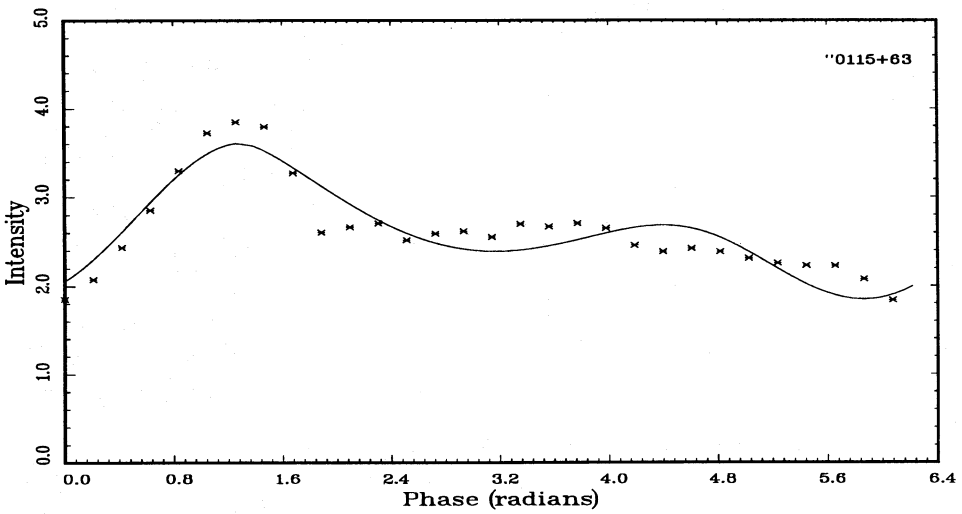

Figure 4. Pulse profiles for the light-bending model.

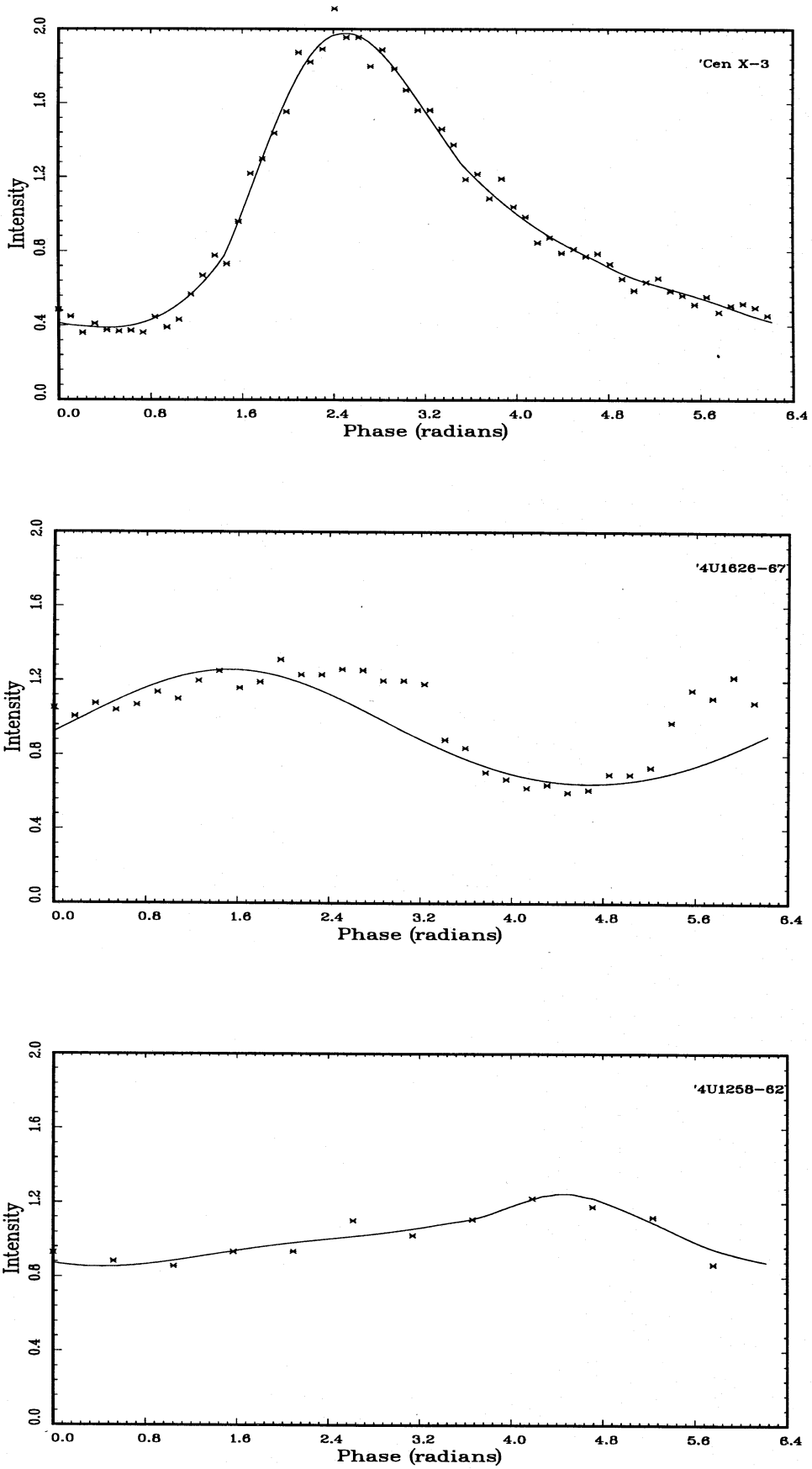

Figure 4 – *continued*

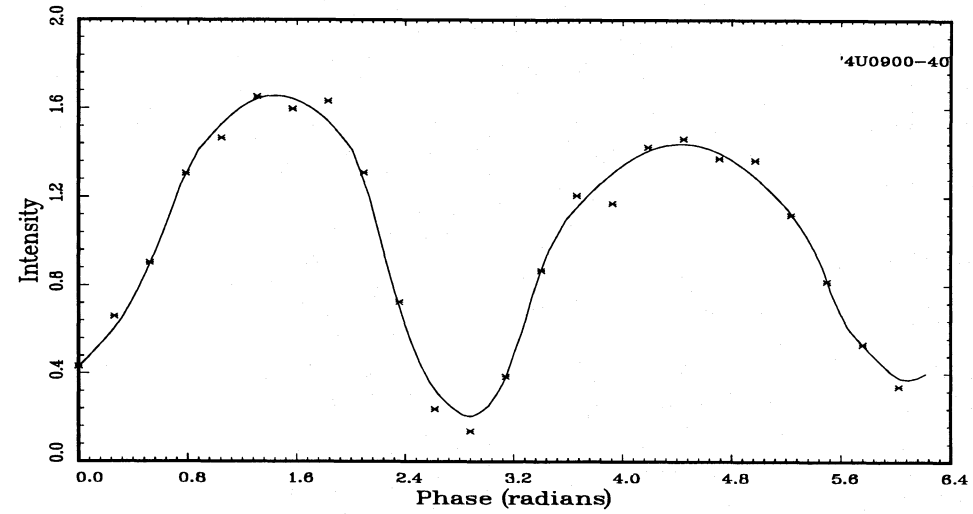

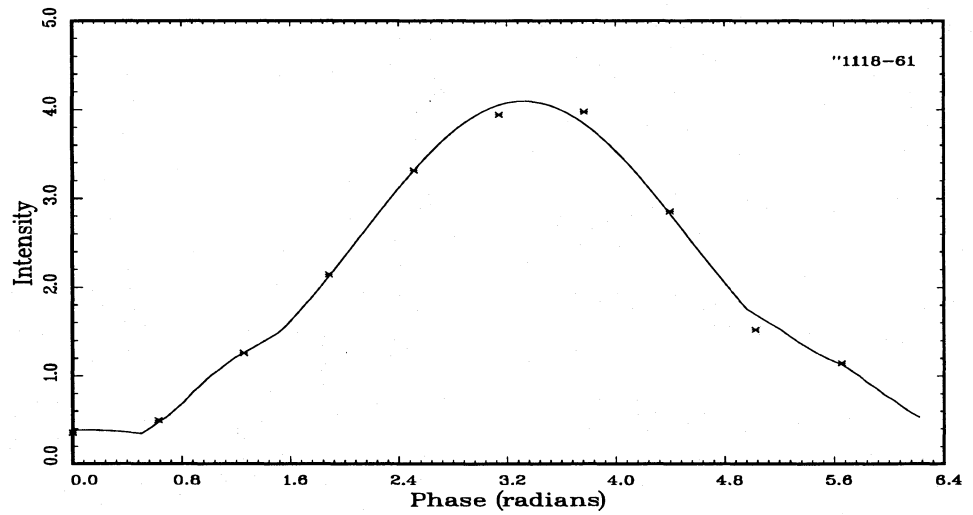

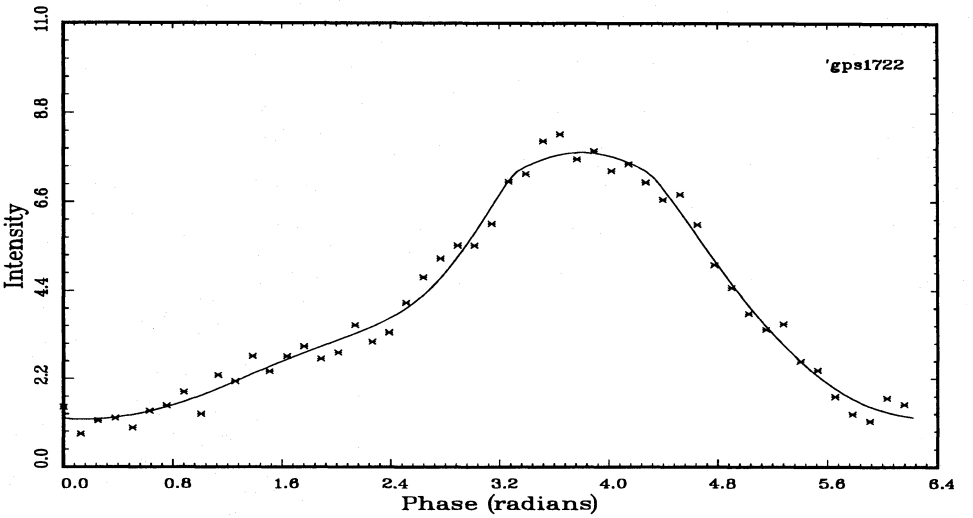

Figure 4 – *continued*

and flow on to a larger region on the neutron star surface. If this assumption is valid, the luminosity-dependent pulse profile can be fitted by varying the size and position of the emission ring, while the other parameters are fixed. So we fix the offset angle θ_o, rotation angle θ_r, and magnetic angle θ_m, and leave the emission ring angles α_1, α_2, β_1 and β_2 free to investigate the dependence of emission region size on the luminosity.

We use the 10 observations from 1985 May 18 to August 13, during which the luminosity decreased from 1.0×10^{38} to 1.2×10^{36} erg s^{-1}. In order to figure out the approximate values which the parameters should be set to, we first leave all 10 parameters free and do the fitting for each of the individual dates independently. Then θ_o, θ_r and θ_m can be set to the average values for the 10 dates to analyse the variations of the emission ring angles with the luminosity.

The observed pulse profiles of EXO 2030+375 have more complicated features than the profiles studied in Section 3. The EXO 2030+375 profiles have some deep notches and sharp peaks which cannot be dealt with by the relatively smooth profiles of the pencil-beam emission model. The 10 parameter-free fits are not very good, and give quite different values of θ_o, θ_r and θ_m for each date. The fits become even poorer after θ_o, θ_r and θ_m are fixed to their average values. Given the bad fittings of emission ring angles α_1, β_1, α_2 and β_2, the study of the correlation between the luminosity and emission rings cannot give satisfactory results.

For many viewing directions, a fan beam can produce sharp features in pulse profile, as the fan beam rotates behind the horizon of the neutron star (Wang & Welter 1981). According to Wang & Frank (1981), when the luminosity is higher than a certain value, possibly around 10^{37} erg s^{-1}, the emission region may switch from a thin slab to a cylindrical 'pillbox'; thus the radiation switches from pencil beam to fan beam. 10^{37} erg s^{-1} is in the range of luminosity observed from EXO 2030+375. Considering the sharp features in the EXO 2030+375 profiles, a fan-beam pattern may be more suitable for this pulsar.

Assuming that the accretion column is a thin-walled hollow funnel, the configuration of the fan-beam model is much more complicated than the flat-ring model. Riffert et al. (1993) made a very simple approximation that the fan-beam model had the same geometry picture as the pencil-beam model, with emission pattern $i=A\ \sin^3\theta$. This is a crude approximation for columns that are small both in height and width. We use this simple fan-beam model to fit the pulse shapes of EXO 2030+375, but the results are less satisfactory than with the pencil-beam model. So EXO 2030+375 is still a mystery. A better geometry figure may improve the fittings and make it possible to investigate the luminosity dependence. From past experience, sometimes simple changes in the model geometry make large differences in the pulse profiles and quality of the fittings.

5 DISCUSSION

Through handling the light-bending equation (equation 3), we found that sometimes a lengthy and complicated equation can be precisely expressed by a very simple one, in a certain region of concern. Replacement of the integral equation (3) with the linear equation (4) not only greatly simplifies the light-bending model, but also makes the light-bending effect itself more straightforward and comprehensible.

From Table 2 we can see that after the effect of the light bending is included, for all of the seven pulsars, the SSQ decreased. The relative decreases range from 0.6 per cent (4U 1626−67) to 76.8 per cent (4U 1118−61); five of the seven pulsars have smaller θ_o; only two θ_os increased; the decreases of θ_o range from 0 per cent (4U 1627−67) to 98.8 per cent (4U 0115+63); for six pulsars, the area of the emission region decreased, from 5.4 per cent (4U 0900−40) to 50.7 per cent (4U 1118−61), the only exception being GPS 1722−36, whose size increased 11.09 per cent.

Generally speaking, with so many parameters, the model fit is not unique. Usually, quite different parameters can be obtained, while the SSQ is not significantly different. In this case, however, although goodness of fit cannot be evaluated, we take the SSQ as a relative measurement of goodness of fit, and the model fit with the smaller SSQ is the better fit. Then we may conclude that the model including the effects of light bending gives significantly better fits to the observations, and geometric pictures more consistent with theoretical estimates.

However, for EXO 2030+375, we conclude that the present model is not applicable, and some mechanisms other than flat emission rings or a simplified fan beam are responsible for the pulse shapes of that pulsar.

REFERENCES

Bulik T., Meszaros P., Woo J., Nagase F., Makashima K., 1992, ApJ, 395, 564
Leahy D. A., 1990, MNRAS, 242, 188
Leahy D. A., 1991, MNRAS, 251, 203
Mészáros P., 1992, High-Energy Radiation from Magnetized Neutron Stars. The University of Chicago Press, Chicago
Mészáros P., Nagel W., 1985, ApJ, 299, 138
Parmar A. N., White N. E., Stella L., 1989a, ApJ, 338, 359
Parmar A. N., White N. E., Stella L., 1989b, ApJ, 338, 373
Riffert H., Mészáros P., 1988, ApJ, 325, 207
Riffert H., Nollert H.-P., Kraus U., Ruder H., 1993, ApJ, 406, 185
Shapiro S. L., Teukosky S. L., 1983, Black Holes, White Dwarfs, and Neutron Stars. Wiley-Interscience, New York
Wang Y.-M., Frank J., 1981, A&A, 93, 255
Wang Y., Welter G., 1981, A&A, 102, 97